CAMBRIDGE
UNIVERSITY PRESS

Research Article

Evolutionary map of the Universe: Detection and analysis of the shell surrounding the runaway Wolf-Rayet star WR16

Aaron Bradley[1], Miroslav D. Filipović[1], Zachary Smeaton[1], Sano Hidetoshi[2,3], Yasuo Fukui[2,4], Cristobal Bordiu[5], Silvina Cichowolski[6], Nick F. H. Tothill[1], Rami Z. E. Alsaberi[2,1], Filomena Bufano[5], Shi Dai[7], Yjan A. Gordon[8], Andrew Hopkins[9], Thomas H. Jarrett[10,1,†], Bärbel S. Koribalski[7,1], Sanja Lazarević[1,7,11], Chris J. Riseley[12], Gavin Rowell[13], Manami Sasaki[14], Dejan Urošević[15] and Tessa Vernstrom[16,17]

[1]Western Sydney University, Penrith South DC, NSW, Australia, [2]Faculty of Engineering, Gifu University, Gifu, Japan, [3]National Astronomical Observatory of Japan, Mitaka, Tokyo, Japan, [4]Department of Physics, Nagoya University, Furo-cho, Chikusa-ku, Nagoya, Japan, [5]INAF –Osservatorio Astrofisico di Catania, Catania, Italy, [6]Instituto de Astronomía y Física del Espacio (UBA, CONICET), CC 67, Buenos Aires, Argentina, [7]Australia Telescope National Facility, CSIRO, Space and Astronomy, Epping, NSW, Australia, [8]Department of Physics, University of Wisconsin-Madison, Madison, WI, USA, [9]School of Mathematical and Physical Sciences, Macquarie University, Sydney, NSW, Australia, [10]Department of Astronomy, University of Cape Town, Rondebosch, South Africa, [11]Astronomical Observatory, Belgrade, Serbia, [12]Astronomisches Institut der Ruhr-Universität Bochum (AIRUB), Bochum, Germany, [13]School of Physical Sciences, The University of Adelaide, Adelaide, Australia, [14]Dr Karl Remeis Observatory, Erlangen Centre for Astroparticle Physics, Friedrich-Alexander-Universität Erlangen- Nürnberg, Bamberg, Germany, [15]Department of Astronomy, Faculty of Mathematics, University of Belgrade, Belgrade, Serbia, [16]CSIRO Space and Astronomy, Bentley, WA, Australia and [17]CRAR, The University of Western Australia, Crawley, Australia

Abstract

We present the first radio–continuum detection of the circumstellar shell around the well-known WN8 type Wolf-Rayet star WR16 at 943.5 MHz using the Australian Square Kilometre Array Pathfinder (ASKAP) Evolutionary Map of the Universe (EMU) survey. At this frequency, the shell has a measured flux density of 72.2±7.2 mJy. Using previous Australia Telescope Compact Array (ATCA) measurements at 2.4, 4.8, and 8.64 GHz, as well as the Evolutionary Map of the Universe (EMU) observations of the star itself, we determine a spectral index of $\alpha = +0.74 \pm 0.02$, indicating thermal emission. We propose that the shell and star both exhibit thermal emission, supported by the its appearance in near-infrared and Hα observations. The latest *Gaia* parallax is used to determine a distance of 2.28±0.09 kpc. This star is well known for its surrounding circular nebulosity, and using the distance and an angular diameter of 8.′42, we determine the shell size to be 5.57±0.22 pc. We use the *Gaia* proper motion (PM) of WR16 to determine peculiar velocities of the star as $V_\alpha(pec) = -45.3\pm5.4$ km s^{-1} and $V_\delta(pec) = 22.8\pm4.7$ km s^{-1}, which indicates that the star is moving in a north-west direction, and translates to a peculiar tangential velocity to be 50.7±6.9 km s^{-1}. We also use these proper motion (PM) to determine the shell's origin, estimate an age of $\sim 9500 \pm 1300$ yr, and determine its average expansion velocity to be 280 ± 40 km s^{-1}. This average expansion velocity suggests that the previous transitional phase is a Luminous Blue Variable (LBV) phase, rather than a Red Super Giant (RSG) phase. We also use the measured flux at 943.5 MHz to determine a mass-loss rate of 1.753×10^{-5} M$_\odot$ yr^{-1}, and use this to determine a lower-limit on ionising photons of $N_{UV} > 1.406 \times 10^{47}$ s^{-1}.

Keywords: Radio continuum emission; Wolf Rayet stars; WN stars; nebulae

1. Introduction

Wolf-Rayet (WR) stars are massive late stage stars with broad emission lines (Crowther 2007). They are categorised by their dominating elemental emission: carbon (WC), nitrogen (WN),

and oxygen (WO). Wolf-Rayet (WR) stars follow an evolutionary cycle that is identifiable by its previous mass–loss history, where mass-loss outbursts are inconsistent unlike O-stars, and caused by internal pulsations (Langer et al. 1994). The previous mass–loss history of these stars is easily identifiable by outbursts of stellar material surrounding them (Nugis & Lamers 2000).

WR16 is a Wolf-Rayet (WR) star of the WN8 type (Shara et al. 2009) at RA (J2000) = 09:54:52.91, Dec (J2000) = −57:43:38.30 (Toalá et al. 2015), which is well known for its ring-like nebula (Cichowolski et al. 2020). While the inner nebula is circular, it is proposed that two more arc-like features outside of this inner nebula share the same origin (Figure 1; Marston 1995). It is likely that winds from the previous O-type star main sequence would have swept the surrounding ISM over several
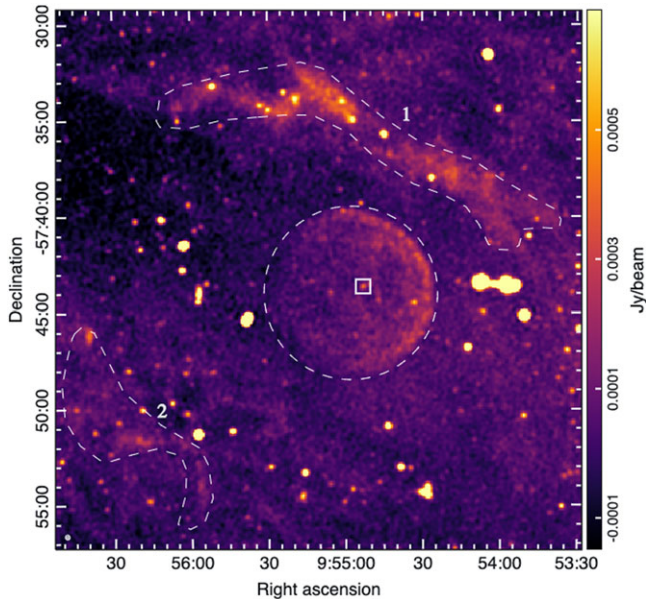
Figure 1. Evolutionary Map of the Universe (EMU) detection of WR16 and its inner shell at 943.5 MHz. The image is linearly scaled and the 15″ beam size is presented by the small white circle in the bottom-left of the image. The white square indicates the position of WR16, the dashed circle shows the position of the 'inner' circular shell. The dashed polygons labelled 1 and 2 indicate the position of 'outer' shell remnants (described in Marston 1995; Cichowolski et al. 2020).

Myrs, creating a wind-blown shell (Langer et al. 1994). Then, after the main sequence, the star would have entered a transitional phase, suffering a number of mass-loss events/outbursts (Crowther 2007). The ejecta from these outbursts would have expanded freely within the cavity carved by the main sequence wind. Finally, when the star became a Wolf-Rayet (WR), the Wolf-Rayet (WR) wind pushed and compressed the ejecta, allowing its most recent outburst to expand symmetrically (Marston 1995).

The Australian Square Kilometre Array Pathfinder (ASKAP) (Hotan et al. 2021) Evolutionary Map of the Universe (EMU) (Norris et al. 2011, 2021; Hopkins et al. 2025) survey is mapping the entire southern sky at 943.5 MHz and is currently ~25% complete. The Australian Square Kilometre Array Pathfinder (ASKAP) telescope has good surface brightness sensitivity that allows us to see characteristics of objects not detected before at this frequency. Previously, extended sources with a similar low-surface brightness to WR16's shell have been characterised such as Supernova Remnants (SNRs); J0624−6948 (Filipović et al. 2022; Sasaki et al. 2025), G288.8−6.3 (Ancora; Filipović et al. 2023; Burger-Scheidlin et al. 2024), G308.7+1.4 (Raspberry; Lazarević et al. 2024a), G312.6+ 2.8 (Unicycle; Smeaton et al. 2024a); and a pulsar wind nebula (PWN) (Potoroo; Lazarević et al. 2024b).

We present an analysis of the star WR16 as seen by Australian Square Kilometre Array Pathfinder (ASKAP) during mapping for the Evolutionary Map of the Universe (EMU) survey. In Section 2, we discuss the observing parameters of the survey, as well as outlining other data used. In Section 3 we explore the results from analysing the Evolutionary Map of the Universe (EMU) tile, as well as exploring the movement of the shell and star, the shell's

expansion, and the presence of a CO bubble. Finally, we give our summary and conclusions in Section 4.

2. Data

2.1. Askap Emu

The object WR16 has been seen in three Australian Square Kilometre Array Pathfinder (ASKAP) Evolutionary Map of the Universe (EMU) observations. SB46953 observed the tile EMU_1017-60 on December 12th 2022, SB51428 observed the tile EMU_0954-55 on July 13th 2023, and SB53568 observed the tile EMU_0936-60 on October 7th 2023. SB46953 is excluded from analysis due to its proximity to the tile's edge, which can cause a drop in sensitivity.

The data were reduced using the standard Australian Square Kilometre Array Pathfinder (ASKAP) pipeline, ASKAPSoft, using multi-frequency synthesis imaging, multi-scale cleaning, self-calibration and convolution to a common beam size (Guzman et al. 2019). As the source was observed in two usable Evolutionary Map of the Universe (EMU) fields, the images were combined with the radio imaging software Miriad (Sault, Teuben, & Wright 1995) using the task IMCOMB. The final image was created by combining the observations with equal weighting. We measure a number of background regions around WR16 to find the background difference in the images. We find a median rms value of 37.5 μJy beam^{-1} and a mean value of 37 μJy beam^{-1}, compared with the previous values of median $= 36$ μJy beam^{-1} and mean $= 43.5$ μJy beam^{-1} (SB51428), and median $= 46.5$ μJy beam^{-1} and mean $= 50.5$ μJy beam^{-1} (SB53568). This background noise level is slightly higher than typical for Evolutionary Map of the Universe (EMU) ($\sigma = 20 - 30$ μJy beam^{-1}; Hopkins et al. 2025), which can be attributed to WR16 being in an area of higher background Galactic emission ($b = -2.55$). The final image is shown in Figure 1 with a resulting sensitivity of $\sigma = 37$ μJy beam^{-1} and a synthesised beam of $15'' \times 15''$.

2.2. Gaia

We use measurements made by the *Gaia* astrometry satellite (Gaia Collaboration et al. 2016) for WR16. We obtain proper motion (PM) and parallax values from Data Release 3 (DR3) (Gaia Collaboration et al. 2023) and use them to determine the star's movement and distance. Discussion surrounding the use of this specific data release is found in Section 3.1.

2.3. Nanten CO

In order to explore the distribution of molecular clouds surrounding WR16, we analysed the archival ^{12}CO($J = 1$–0) data taken by the NANTEN 4-m radio telescope (Mizuno & Fukui 2004). The angular resolution of the data cube was $2.'6$. The typical noise fluctuations were ~0.3 K at a velocity resolution of 0.65 km s^{-1}.

2.4. Other data

We include observations from the SuperCOSMOS (Hambly et al. 2001) and Wide-Field Infrared Survey Explorer (WISE) (Wright et al. 2010) sky surveys to compare the nebulosity surrounding WR16 at 656.281 nm and 22 μm (Figure 2).

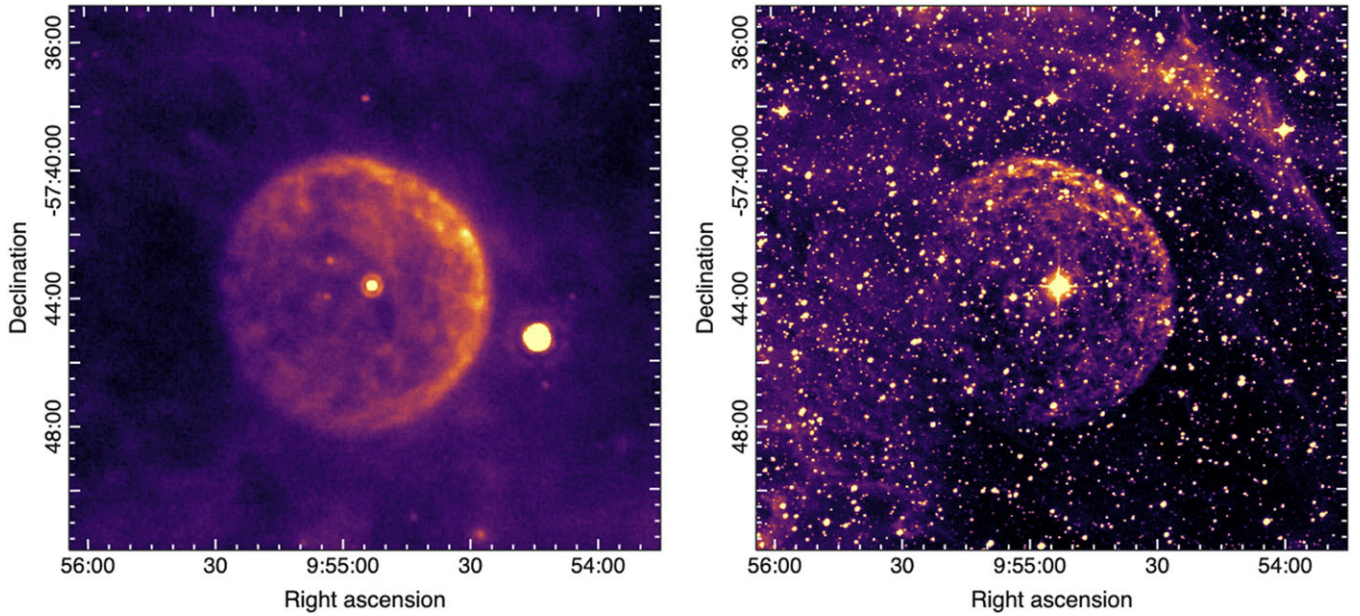**Figure 2.** Detection of WR16 and its shell at 22 μm from and Wide-Field Infrared Survey Explorer (WISE) infrared (Left), and SuperCOSMOS Hα (Right). Both sub-images are linearly scaled.

Table 1. Measured flux densities of the Wolf-Rayet star WR16 and its nebulous shell.

	S^a_{944}	$S^b_{2.40}$	$S^c_{4.80}$	$S^c_{8.64}$	α
WR16	(mJy)	(mJy)	(mJy)	(mJy)	$\alpha \pm \Delta\alpha$
Star	0.35±0.04	0.69±0.15	1.21±0.09	1.75±0.09	0.74±0.02
Shell	72.2±7.2	–	–	–	–

[a] Measurements made as part of this paper.
[b] Measurements using Australia Telescope Compact Array (ATCA) observations from Chapman et al. (1999).
[c] Measurements using Australia Telescope Compact Array (ATCA) observations from Leitherer et al. (1995).

We also use previous flux density measurements using Australia Telescope Compact Array (ATCA) from Leitherer et al. (1995), Leitherer et al. (1997), and Chapman et al. (1999). These measurements are included in Table 1, and discussed in Section 3.1.

We have searched for high-energy associations to WR16 and its shell. Fermi-LAT Data Release 4 (Abdollahi et al. 2022; Ballet et al. 2023) shows no corresponding Gamma-Ray emission. The SRG/eROSITA all-sky survey (eRASS) Data Release 1 (Merloni et al. 2024), and observations taken with *XMM-Newton* (Strüder et al. 2001; Turner et al. 2001) show no corresponding X-Ray emission.

3. Results and discussion

3.1. Measurements

Using a *Gaia* parallax of 0.4380±0.0168 mas (Gaia Collaboration 2020), we estimate the distance of WR16 to be 2.28±0.09 kpc. This is in accordance with the photometric distance calculated in van der Hucht (2001) of 2.37 kpc, and with a distance of 2.23±0.39 kpc derived using Ca II lines (Megier et al. 2009). Previously, *Gaia* Data Release 2 (DR2) (Gaia Collaboration 2018) provided a distance of 2.66±0.23 kpc (Bailer-Jones et al. 2018). Considering that *Gaia* DR3 provides a distance that is concordant with other measurements, we adopt 2.28±0.09 kpc to be the most accurate distance value.

We obtain proper motion (PM) from *Gaia* DR3 (Gaia Collaboration 2020), for WR16, which are μ_α: -9.458 ± 0.021 mas yr^{-1} and μ_δ: 5.054 ± 0.018 mas yr^{-1}. Using the Gaia parallax and proper motion values, we calculate the peculiar velocity with respect to the local interstellar medium following Comerón & Pasquali (2007) and Cichowolski et al. (2020). We determine the stellar peculiar velocity to be $V_\alpha(pec) = -45.3\pm5.4$ km s^{-1} and $V_\delta(pec) = 22.8\pm4.7$ km s^{-1}, indicating that the star is moving in a north-west direction, which is discussed further in Section 3.3. This matches the brighter north-western component of the circular nebulosity observed in radio, infrared, and Hα (Figures 1 and 2). We then calculate the peculiar tangential velocity to be 50.7±6.9 km s^{-1}.

We measure the inner WR16 nebula to have a flux density of 72.2±7.2 mJy at 943.5 MHz, taking an error of 10% (as discussed in Smeaton et al. 2024b; Filipović et al. 2024). We also measure the flux density of the central star at 943.5 MHz, and find it to be 0.35±0.04 mJy. We combine this with the Australia Telescope Compact Array (ATCA) flux density measurements listed in Table 1 and Section 2.4 to compute a spectral index for the star (See Figure 3). The radio spectral index is defined as $S \propto \nu^\alpha$, where S is flux density, ν is the frequency and α is the spectral index. We calculate the spectral index using the LINREGRESS[a] function in the Python SCIPY (Virtanen et al. 2020) library. The function uses the linear least-squares regression method to find a best fit line of $\alpha = +0.74 \pm 0.02$ for WR16. This is very close to the canonical spectral index of an isothermal, spherical stellar wind ($\alpha = +0.6$, Panagia & Felli 1975; Wright & Barlow 1975),
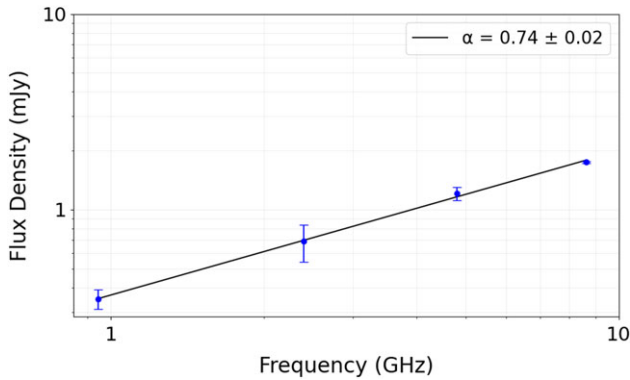
[a] https://docs.scipy.org/doc/scipy/reference/generated/scipy.stats.linregress.html

Figure 3. Spectral index plot of WR16 star, using flux density values from Table 1.

and is similar to that of Dougherty & Williams (2000) for similar Wolf-Rayet (WR) stars that also exhibit thermal characteristics.

We fit a circular region to the outer edge of the shell and measure an angular diameter of 8.′42, which is similar to the angular size estimated in Cichowolski et al. (2020). We use the derived distance and the angular size measured on the Evolutionary Map of the Universe (EMU) image (Figure 1) to determine the shell's true linear size and find that the shell has a diameter of 5.57±0.22 pc. Due to the shell's presence in near–infrared and Hα (Figure 2) we infer that the shell also has thermal origin. Because the shell has not yet been observed at other frequencies, we cannot confirm thermal origin from the spectral index.

3.2. Large-scale wind-blown bubble of CO

Figure 4(a) shows the velocity-integrated intensity map of CO toward WR16 with an integration range of from −7 to 0 km s^{-1}. We found a new candidate for a large-scale wind-blown bubble whose radius is approximately 0.°75 or ∼30 pc at the distance of WR16. Since the inner circular shell of WR16 is approximately placed at the geometric center of the CO bubble, they appear to be physically associated to each other.

Figure 4(b) and (c) show the position–velocity diagrams of CO. We found clear evidence of an expanding gaseous bubble whose expanding velocity is ∼7 km s^{-1}. The fact that the spatial extent in the Declination direction on the position–velocity diagram varies depending on the integrated Right Ascension range is also roughly consistent with the three-dimensional expansion motion of the molecular clouds.

We argue that the dynamical timescale of this expanding gaseous bubble can be naturally understood if it is assumed to have been driven by WR16. The dynamical time scale of the expanding bubble is estimated to be (bubble radius)/(expanding velocity) ∼30 pc/7 km s^{-1} ∼ 4 Myr. This time scale is roughly consistent with the typical lifetime of a massive star, suggesting that the CO expanding bubble was likely formed by stellar feedback effects such as strong stellar winds from the progenitor of WR16.

3.3. Shell expansion

Figure 5 shows several on-image measurements of the shell surrounding WR16. We find that the tangential peculiar velocity of the star passes through the geometric center of the 8.′42 circle (RA (J2000) = 09:54:57.8, Dec (J2000) = −57:43:58.9), as indicated by the dashed black line in the figure. The distance of the star to the center of the nebulosity is 44.″81. We convert this distance from

angular size to linear size (0.49 pc, or 1.53×10^{13} km), and multiply the calculated velocity in Section 3.1 by seconds in a year (3.154×10^7 s) to obtain a yearly velocity of 1.58×10^9 km yr^{-1}, 5.12×10^{-5} pc yr^{-1}. We can determine the amount of time it has taken for WR16 to travel to its current point by dividing the linear size by the yearly velocity, and return a value of ∼ 9 500 ± 1 300 yr.

Assuming that the shell originated at the point that WR16 passed through its geometric centre coordinates, we can measure its average expansion velocity based on the distance travelled by WR16. The radius of the shell is 4.′21, which converts to a linear size of 8.62×10^{13} km (2.79 pc). Dividing this by the years travelled (∼ 9 500 ± 1 300 yr) and dividing by seconds in a year, we determine the average expansion velocity of the circular shell to be 280 ± 40 km s^{-1}. It is important to note that this only assumes a 2–dimensional plane, and is therefore a lower limit on age values and an upper limit on expansion values.

We take our calculated expansion velocity to be the average rate of expansion because it is presumed that the shell is slowing down the more it expands and interacts with the surrounding interstellar medium. WR16 also has a wind terminal velocity (v_∞) of 630 km s^{-1} (Toalá et al. 2015), so it is likely that the wind-driven shell started with velocities similar to this, and has slowed over the ∼ 9 500 ± 1 300 yr timescale. This velocity sits conveniently between the typical expansion speed of Luminous Blue Variable (LBV) shells of ∼50 km s^{-1} (Weis 2011), like that of AG Car (Smith 1991), and the faster ejecta of Eta Car (600 km s^{-1}, Steffen et al. 2014). This supports the idea that the shell originated in a previous Luminous Blue Variable (LBV) phase.

3.4. Mass-loss rate

Based on the observed parameters of WR16 at 943.5 MHz, we are able to determine a mass-loss rate ($\dot{M}$) at this frequency using the equations outlined in (Wright & Barlow 1975, Equation 20) and (Leitherer et al. 1995, Equation 3). We calculate a Gaunt factor, g_v, at 943.5 MHz to be 5.99, assuming a gas temperature of 10^4 K and a Z of 1. Using the same constants for our calculation as Leitherer et al. (1995), and substituting our flux, distance, and frequency, we derive a mass-loss rate of 1.753×10^{-5} M$_\odot$ yr^{-1}.

This is lower than the calculated mass-loss rate from Leitherer et al. (1995) of 3.981×10^{-5} M$_\odot$ yr^{-1}. However, recalculating their value using our *Gaia* distance measurement of 2.28 kpc, we get a result of 2.188×10^{-5} M$_\odot$ yr^{-1}. These measurements are quite similar, and may indicate that the mass-loss rate has decreased slightly over the 30 yr between observations. It is also important to note that the canonical value for mass-loss rates in WN8 stars like WR16 (Section 1) is 1.995×10^{-5} M$_\odot$ yr^{-1} (Crowther 2007).

Using the calculated mass-loss rate, we are also able to determine a lower limit of ionising photons that WR16 are released per second as in (Wright & Barlow 1975, Equation 23). We use a radius of 19 R$_\odot$ (Schmutz, Hamann, & Wessolowski 1989) to calculate a lower limit value of $N_{UV} > 1.406 \times 10^{47}$ s^{-1}, which is in concordance with the canonical value for WN8 stars of 1.259×10^{49} s^{-1} (Crowther 2007).

3.5. Similarities to other objects

WR16 presents an almost symmetrical circular shell similar to the Galactic Supernova Remnants (SNRs) Teleios (Greek τελειος – meaning perfect, Filipović et al. submitted). Although they share
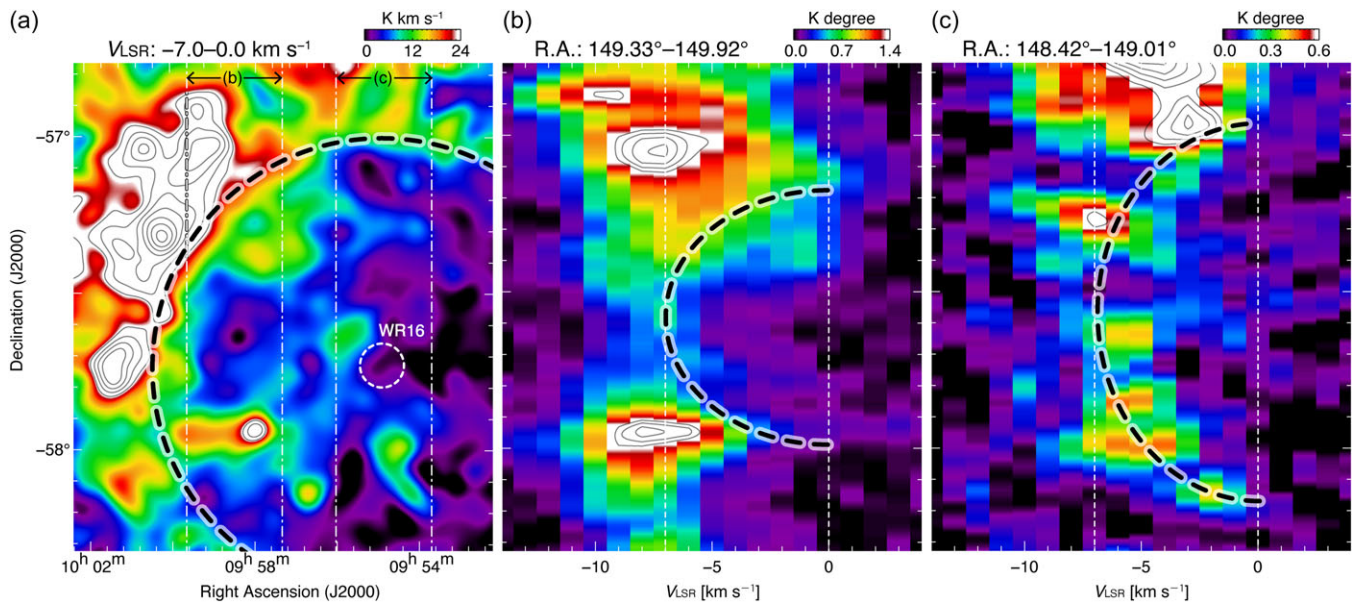
Figure 4. (a) – Distribution of the NANTEN ^{12}CO($J = 1$–0) line emission toward WR16 (Mizuno & Fukui 2004). The integration velocity range is from -7 to 0 km s^{-1}. The incomplete circular shell indicates a wind-blown bubble detected in CO (see Section 3.2). The dashed circle shows the position of the inner circular shell of WR16. (b,c) – Position–velocity diagrams of CO. The integration range of Right Ascension is from 149°33 to 149°92 for (b) and from 148°42 to 149°01 for (c). The dashed semicircles represent the expanding motion of CO due to the stellar wind from WR16 (see Section 3.2).
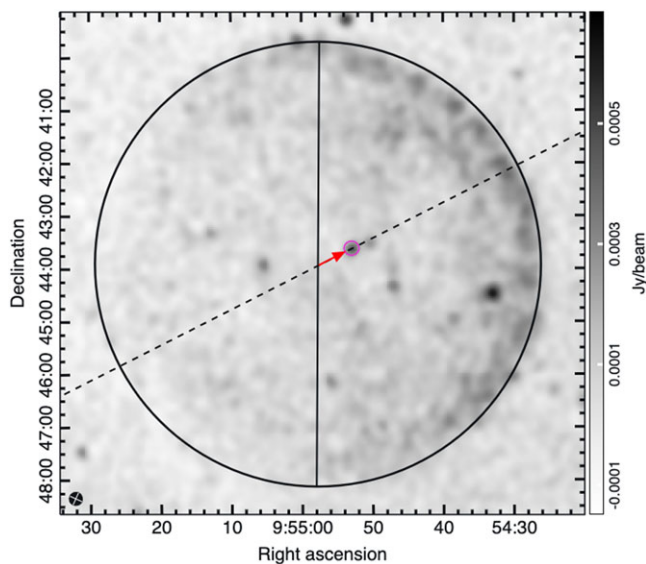
Figure 5. Measurements of the circular nebulosity surrounding WR16 and peculiar velocity mapped over the EMU image, similar to Figure 1. The 8′42 diameter shell is shown as a black circle. The magenta circle indicates the position of WR16, and the red arrow shows its distance from the shell's geometric center, as well as its direction. The black dashed line represents the projected path of WR16's peculiar velocity, which points toward the north-west (top-right).

similarities, they are unique objects for their given type. This shows that different objects can share the same morphologies, and can possibly be equated to similar formation processes.

Another object similar to the WR16 shell is the radio ring Kýklos, discussed in Bordiu et al. (2024). They discuss the likelihood of the ring-like object being an outburst of a Wolf-Rayet (WR) star. This object is also situated in our Galaxy, but is significantly smaller than WR16 (WR16: 8′42, Kýklos: 80″). Both

systems show evidence of thermal emission, however, Kýklos presents a ring-like structure rather than a diffuse circle like WR16. The ring-like structure and smaller size may indicate that Kýklos is at an earlier developmental stage compared to WR16.

We see significant brightening toward the north–west part of the WR16 circular shell. This is likely due to the closer proximity of WR16, which also explains the much fainter south–east portion. This edge brightening is similar to the Lagotis H II region discussed in Bradley et al. (2025). In the case of Lagotis, edge brightening is caused by a cluster moving into a molecular cloud, whereas for WR16, it can be seen as the star catching up with its shell edge.

4. Conclusion

We present the detection of the nebulosity surrounding the Wolf-Rayet star WR16 and its circular shell at 943.5 MHz using the ASKAP EMU survey. We find that the shell has a measured flux density of 72.2 ± 7.2 mJy, and WR16 has a flux density of 0.35 ± 0.04 mJy. By combining this with archival Australia Telescope Compact Array (ATCA) data, we determine a spectral index of $+0.74 \pm 0.02$ for the star, which indicates thermal origin of the emission. We also infer that the shell is thermal from its presence in IR and Hα. We use *Gaia* DR3 measurements to determine the star's direction and distance. WR16 is moving in a north-western direction, coinciding with the brighter edge of the nebulosity.

We also find that the star is at a distance of 2.28 ± 0.09 kpc, and measure the shell to be 8′42 in angular diameter, which translates to a linear size of 5.57 ± 0.22 pc. The shell as seen by Evolutionary Map of the Universe (EMU) matches well with Wide-Field Infrared Survey Explorer (WISE) and SuperCOSMOS data, further confirming thermal emission. By mapping proper motion (PM), we are able to determine the origin point of the shell and calculate the age of the shell to be $\sim 9\,500 \pm 1\,300$ yr, with an

average expansion velocity of 280 ± 40 km s^{-1}. It is expected that the brighter edge of the shell will become brighter as WR16 moves towards it.

We also discuss the discovery of a large wind-blown bubble seen in CO observations, which is proposed to be related to WR16 during its main-sequence phase. We calculate a mass-loss rate of 1.753×10^{-5} M$_\odot$ yr^{-1}, which is remarkably close to the canonical value of the mass-loss rate for WN8 type stars. Using this we were able to determine the amount of UV-ionising photons emanating from WR16: $N_{UV} > 1.406 \times 10^{47}$ s^{-1}.

References

Abdollahi, S., et al. 2022, ApJS, 260, 53

Bailer-Jones, C. A. L., Rybizki, J., Fouesneau, M., Mantelet, G., & Andrae, R. 2018, AJ, 156, 58

Ballet, J., Bruel, P., Burnett, T. H., Lott, B., & The Fermi-LAT Collaboration. 2023, arXiv e-prints, arXiv:2307.12546

Bordiu, C., et al. 2024, A&A, 690, A53

Bradley, A. C., et al. 2025, PASA, e032

Burger-Scheidlin, C., et al. 2024, A&A, 684, A150

Chapman, J. M., Leitherer, C., Koribalski, B., Bouter, R., & Storey, M. 1999, ApJ, 518, 890

Cichowolski, S., et al. 2020, MNRAS, 495, 417

Comerón, F., & Pasquali, A. 2007, A&A, 467, L23

Crowther, P. A. 2007, ARA&A, 45, 177

Dougherty, S. M., & Williams, P. M. 2000, MNRAS, 319, 1005

Filipović, M. D., et al. 2022, MNRAS, 512, 265

Filipović, M. D., et al. 2023, AJ, 166, 149

Filipović, M. D., et al. 2024, PASA, 41, e112

Gaia Collaboration. 2018, VizieR Online Data Catalog: Gaia DR2 (Gaia Collaboration, 2018), VizieR On-line Data Catalog: I/345. Originally published in: 2018A&A...616A...1G, doi: 10.26093/cds/vizier.1345

Gaia Collaboration. 2020, VizieR Online Data Catalog: Gaia EDR3 (Gaia Collaboration, 2020), VizieR On-line Data Catalog: I/350. Originally published in: 2021A&A...649A...1G, doi: 10.26093/cds/vizier.1350

Gaia Collaboration, et al. 2016, A&A, 595, A1

Gaia Collaboration, et al. 2023, A&A, 674, A1

Guzman, J., et al. 2019, ASKAPsoft: ASKAP science data processor software, Astrophysics Source Code Library, record ascl:1912.003

Hambly, N. C., et al. 2001, MNRAS, 326, 1279

Hopkins, A. M., et al. 2025, arXiv e-prints, arXiv:2505.08271

Hotan, A. W., et al. 2021, PASA, 38, e009

Langer, N., et al. 1994, A&A, 290, 819

Lazarević, S., et al. 2024a, RNAAS, 8, 107

Lazarević, S., et al. 2024b, PASA, 41, e032

Leitherer, C., Chapman, J. M., & Koribalski, B. 1995, ApJ, 450, 289

Leitherer, C., Chapman, J. M., & Koribalski, B. 1997, ApJ, 481, 898

Marston, A. P. 1995, AJ, 109, 1839

Megier, A., Strobel, A., Galazutdinov, G. A., & Krełowski, J. 2009, A&A, 507, 833

Merloni, A., et al. 2024, A&A, 682, A34

Mizuno, A., & Fukui, Y. 2004, in Astronomical Society of the Pacific Conference Series, Vol. 317, Milky Way Surveys: The Structure and Evolution of our Galaxy, ed. D. Clemens, R. Shah, & T. Brainerd, 59

Norris, R. P., et al. 2011, PASA, 28, 215

Norris, R. P., et al. 2021, PASA, 38, e046

Nugis, T., & Lamers, H. J. G. L. M. 2000, A&A, 360, 227

Panagia, N., & Felli, M. 1975, A&A, 39, 1

Sasaki, M., et al. 2025, A&A, 693, L15

Sault, R. J., Teuben, P. J., & Wright, M. C. H. 1995, in Astronomical Society of the Pacific Conference Series, Vol. 77, Astronomical Data Analysis Software and Systems IV, ed. R. A. Shaw, H. E. Payne, & J. J. E. Hayes, 433

Schmutz, W., Hamann, W. R., & Wessolowski, U. 1989, A&A, 210, 236

Shara, M. M., et al. 2009, AJ, 138, 402

Smeaton, Z. J., et al. 2024a, RNAAS, 8, 158

Smeaton, Z. J., et al. 2024b, MNRAS, 534, 2918

Smith, L. J. 1991, in IAU Symposium, Vol. 143, Wolf-Rayet Stars and Interrelations with Other Massive Stars in Galaxies, ed. K. A. van der Hucht, & B. Hidayat, 385

Steffen, W., et al. 2014, MNRAS, 442, 3316

Strüder, L., et al. 2001, A&A, 365, L18

Toalá, J. A., Guerrero, M. A., Ramos-Larios, G., & Guzmán, V. 2015, A&A, 578, A66

Turner, M. J. L., et al. 2001, A&A, 365, L27

van der Hucht, K. A. 2001, NewAR, 45, 135

Virtanen, P., et al. 2020, NM, 17, 261

Weis, K. 2011, in IAU Symposium, Vol. 272, Active OB Stars: Structure, Evolution, Mass Loss, and Critical Limits, ed. C. Neiner, G. Wade, G. Meynet, & G. Peters, 372

Wright, A. E., & Barlow, M. J. 1975, MNRAS, 170, 41

Wright, E. L., et al. 2010, AJ, 140, 1868